Accepted Manuscript

The influence of Al_2O_3 particle morphology on the coating formation and dry sliding wear behavior of cold sprayed Al-Al_2O_3 composites

J.M. Shockley, S. Descartes, P. Vo, E. Irissou, R.R. Chromik

PII: S0257-8972(15)00091-2
DOI: doi: 10.1016/j.surfcoat.2015.01.057
Reference: SCT 20072

To appear in: *Surface & Coatings Technology*

Received date: 14 November 2014
Accepted date: 22 January 2015

Please cite this article as: J.M. Shockley, S. Descartes, P. Vo, E. Irissou, R.R. Chromik, The influence of Al_2O_3 particle morphology on the coating formation and dry sliding wear behavior of cold sprayed Al-Al_2O_3 composites, *Surface & Coatings Technology* (2015), doi: 10.1016/j.surfcoat.2015.01.057

This is a PDF file of an unedited manuscript that has been accepted for publication. As a service to our customers we are providing this early version of the manuscript. The manuscript will undergo copyediting, typesetting, and review of the resulting proof before it is published in its final form. Please note that during the production process errors may be discovered which could affect the content, and all legal disclaimers that apply to the journal pertain.

ACCEPTED MANUSCRIPT

The influence of Al_2O_3 particle morphology on the coating formation and dry sliding wear behavior of cold sprayed Al-Al_2O_3 composites

J. M. Shockley[1], S. Descartes[1,2], P. Vo[3], E. Irissou[3], R.R. Chromik[1]*

1 Department of Mining and Materials Engineering, Aluminum Research Centre – REGAL, McGill University, M.H. Wong Building, 3610 University Street, Montreal, QC H3A 0C5, Canada

2 Université de Lyon, CNRS, INSA-Lyon, LaMCoS, UMR5259, 69621 Villeurbanne, France

3 National Research Council Canada, 75, boul. de Mortagne, Boucherville, QC J4B 6Y4, Canada

* corresponding author email: richard.chromik@mcgill.ca

Abstract

Five Al-Al_2O_3 coatings were deposited by gas dynamic cold spray, using feedstocks containing 0, 10, and 50 wt.% of Al_2O_3 particles admixed into commercially pure Al powders. Two feedstocks were made using Al_2O_3 powders with an angular, blocky Al_2O_3 morphology, two feedstocks used Al_2O_3 powders with a spherical morphology, and the fifth consisted of 100% Al. The influence of Al_2O_3 concentration and morphology in the feedstock powders on the cold spray coating formation was measured in terms of Al_2O_3 recovery in the coatings, deposition efficiency, and microstructural analysis. The Al-Al_2O_3 coatings were then subjected to dry sliding wear experiments from which the friction, wear, and microevolution of third body structures in the wear track and transfer film were observed. The spherical Al_2O_3 morphology was associated with improved tribological behavior compared to the angular morphology when comparing similar coating concentrations of Al_2O_3.

1 Introduction

Aluminum matrix composite (Al-MMC) materials with hard reinforcements are valued for their corrosion resistance, low density, and improved wear resistance over the unreinforced alloy materials [1]. Depending on the processing route and application, the reinforcement phase may consist of long fibers, short fibers, or particulates, and are often based on SiC or Al_2O_3, among other materials [2]. Particulate-reinforced Al-MMC materials may be produced through bulk

ACCEPTED MANUSCRIPT

processing or applied as coatings, and have been found to have substantially lower wear rates compared to the un-reinforced matrix alloy in most wear regimes [2-6].

Although thermal spray routes are the most conventional choice for depositing Al-MMC coatings, a more recent alternative is the cold gas dynamic spray technique, more often known as cold spray [5, 7-9]. The cold spray process operates by accelerating feedstock powders through a preheated inert gas stream that is passed through a de Laval-type nozzle. The gas and powders attain supersonic velocities, and upon impact with a substrate, extensive plastic deformation is induced and metallurgical bonding takes place by way of adiabatic shear instability [10-14]. In-flight chemical reactions and substrate heating during cold spray are minimal compared to conventional thermal spray processes because of the lower gas temperatures. Furthermore, the high velocities during deposition lead to a very high density in the cold sprayed deposits [10]. Cold spray of pure aluminum and Al-MMC materials has become a mode of repair and corrosion protection for magnesium aerospace gearbox components, among other applications [9, 15].

To produce Al-MMC coatings by cold spray, reinforcement particles are admixed into the feedstock powder, and during deposition some particles are recovered into the final coating. Hard reinforcement particles do not participate in the adiabatic shear instability process, so the particles must embed themselves in the coating during formation and the recovery of hard particles may be less than in the initial feedstock [5, 7]. The commonly available Al_2O_3 powders are fused and crushed, which are dense with no internal porosity and have blocky, angular morphologies. One means of modifying the Al_2O_3 particle morphology is by post-treating angular Al_2O_3 by way of a plasma spheroidization process. Previous studies by the authors explored the dry sliding wear behavior and wear mechanisms of cold sprayed Al-Al_2O_3 composite coatings using the angular morphology [6, 16]. In these studies, the role of angular Al_2O_3 particles in the tribological processes was explained through the use of *in situ* tribometry and microanalysis of the “third bodies," which are the mechanically modified structures formed at the sliding interface [17]. However, given the commercial availability of both angular and spherical Al_2O_3 particle morphologies, understanding the inuence of Al_2O_3 morphology in the cold spray deposition process and tribological behaviors of cold sprayed Al-Al_2O_3 is of potential significance to the coatings industry.

ACCEPTED MANUSCRIPT

In the present study, the influence of Al_2O_3 particle morphology on the cold spray deposition and subsequent dry sliding wear behavior of Al-Al_2O_3 coatings is explored. Two Al_2O_3 powders, one angular and one spherical, were admixed into commercially pure Al powder at varying concentrations and the powder mixtures were cold sprayed at similar deposition conditions. Analysis of deposition efficiency was conducted through in situ monitoring of powder flow rates, and Al_2O_3 recovery in the coating was analyzed through microstructural analysis. Then dry sliding wear tests were conducted against a sapphire counterface, by which the evolution of wear rate, frictional forces, and the subsurface microstructure were studied. Through the study of cold spray deposition behavior, coating microstructure, and dry sliding wear behavior, a discussion of the implications of Al_2O_3 morphology will be developed.

2 Experimental Methods

2.1 Cold spray deposition and coating characterization

Four batches of feedstock powder were prepared by admixing commercially available spherical Al powder (Valimet H-15, d50= 22.57 µm) with 10 and 50 wt.% of either angular morphology Al_2O_3 powder (Plasmatec, d50= 25.5 µm) or a plasma spheroidized spherical morphology Al_2O_3 powder (Tekna, d50 = 24.26 µm) (see Figure 1). Coatings were deposited onto aluminum alloy AA6061 substrates using a Plasma Giken PCS-800 cold spray system, achieving a thickness of 4-5 mm. A nitrogen carrier gas was used at a 400° chamber temperature and 3 MPa chamber pressure. The 76.2 mm wide substrates were kept stationary and the gun nozzle moved at a 200 mm/s traverse speed with a 1 mm step size. Powder consumption was monitored in situ using digital scales upon which the powder hopper was mounted. Deposition efficiency was calculated by dividing the total mass of the deposited coating by the mass of powder sprayed.

Cross-sections of each coating were prepared for analysis by sectioning using a diamond wafering saw, cold mounting in epoxy, fine grinding using 400, 800, 1200, and 2400 grit sizes, and polishing using 9 µm, 3 µm and 1 µm diamond pastes followed by 0.05 µm colloidal silica. The concentration of Al_2O_3 recovered in each coating was measured by image analysis, during which ten random backscattered electron (BSE) images at 700x magnification of polished cross-sections were taken in a scanning electron microscope (SEM) and analyzed by pixel count to calculate the volumetric Al_2O_3 concentration, which was converted to mass concentration. Prior

ACCEPTED MANUSCRIPT

to wear testing, the coating surfaces were subjected to fine grinding and cleaned with ethanol. The root mean square roughness value fell between 0.4 and 0.8 μm for all samples after preparation. Microhardness measurements were taken using a Vickers indenter applied at a 200 gf (1.96 N) load with a hold time of 5 seconds, and each hardness value reported here shows the average of at least ten indents taken at random locations on the polished coatings.

2.2 Sliding wear test conditions

Sliding wear tests on the prepared coatings were performed in dry air (below 1% relative humidity) at room temperature (21-24° C). All tests were conducted with a sliding speed of 3 mm/s, a track length of 10 mm, and normal load of 1 N. Friction forces were measured at a sampling rate of 800 Hz using a piezoelectric sensor mounted underneath the sample stage. Monocrystalline a-Al_2O_3(sapphire) spheres (or hemispheres for in situ tests) of 6.35 mm diameter were used as the counterface material. Wear tests were run to 50, 500 and 2000 sliding cycles, corresponding to total sliding distances of 0.5, 5, and 20 m, respectively. Three repeats were used for the 50 and 500 cycle condition, while two repeats were used for the 2000 cycle condition. One 500-cycle test per coating was performed in the in situ configuration, in which microscopic observation of the contact region was carried out through the transparent hemispherical counterface using an optical microscope [6, 16, 18]. For this purpose, the microscope was mounted above the counterface and was equipped with a 10x objective lens and a commercially available camcorder. The use of the in situ configuration was not found to influence the friction or wear rate behavior compared to the conventional configuration.

2.3 Analysis of wear tracks

Using an SEM, wear track surface features were observed and elemental contrast was revealed by energy dispersive x-ray spectroscopy (EDXS). Surface morphologies of the wear tracks and counterface transfer material were extracted using a Wyko NT8000 optical interferometer. Wear rates were calculated in accordance with ASTM Standard G99 by first integrating height profiles across the wear track above and below the original surface height to calculate a net worn cross-sectional area. This was then multiplied by the wear track length to obtain a net volume of material removed from the surface. Between 80-100 surface profile measurements per wear track were obtained.

ACCEPTED MANUSCRIPT

Sub-surface regions of the worn surfaces were revealed by cross-sectioning. Wear tracks were cut transverse to the sliding direction using a lubricated slow-speed abrasive cutting wheel, followed by cold mounting in epoxy and mechanical polishing. Microstructural analysis was carried out in an SEM with a backscattered electron detector to reveal aluminum grains through electron channeling contrast imaging (ECCI).

Nanoindentation was performed on wear track cross-sections and directly on wear track surfaces using a Hysitron Triboindenter equipped with a Berkovich diamond indenter with a tip defect radius of approximately 125 nm. Indents were performed using a 5 second loading time to a maximum force of either 400 or 2000 μN, a 5 second hold time at maximum load, and a 5 second unloading time. To precisely control the location of the indents, the Berkovich indenter was used to collect *in situ* scanning probe microscopy (SPM) images that were matched to previously acquired electron micrographs of the areas of interest. Each hardness value reported was calculated using the Oliver and Pharr method [19], and represents the average of at least 8 indents.

3 Coating formation

The recovery of Al_2O_3 varied according to the feedstock content and Al_2O_3 particle morphology (see Table 1 and Figure 2). The angular Al_2O_3 recovery was similar to that measured in previous studies, in spite of the use of different cold spray guns and deposition velocities [5,7]. The amount of recovery of spherical Al_2O_3 was considerably lower than the amount of recovery of angular Al_2O_3. The deposition efficiency (DE) of the 10 wt.% Al_2O_3 feedstock powder was unchanged from that of the pure Al powder for the angular Al_2O_3 morphology and slightly higher for the spherical morphology. The DE of both 50 wt.% Al_2O_3 feedstock powders was significantly lower for both morphologies (see Figure 2).

In cold spray of pure metals, coating formation has been attributed to plastic deformation at the interface of the impacting particle, which leads to “jetting" of the interfacial material and metallurgical bonding by way of adiabatic shear instabilities [10-14]. Thus a hard elastic secondary phase, in this case Al_2O_3, is not believed to participate in this aspect of the coating process due to its lack of plasticity in this temperature range. When hard ceramics are cold sprayed alone, they behave erosively and no coating is formed [5, 20]. When admixed into Al

ACCEPTED MANUSCRIPT

powder, they can be recovered in the coating, but generally the coating contains a lower hard particle content than the feedstock powder [5]. The results presented in Figure 2 showed lower Al_2O_3 concentration than their feedstock powders, with the exception of ANG10, which had roughly the same amount. This Al_2O_3 recovery behavior is consistent with that observed in previous studies [5,7]. The change of deposition efficiency as a function of feedstock Al_2O_3 has also been previously observed, where at lower Al_2O_3 contents it can be beneficial to the DE, but beyond a certain point is detrimental [5, 21]. The initial benefit to DE may be attributed to peening and cleaning of the surface by the hard particles, but at higher concentrations, the DE is lowered through erosive behavior and a lack of bonding between Al_2O_3 particles.

The lower recovery of spherical Al_2O_3 compared to the angular morphology can be partly explained by modelling and experimental work by Getu et al. [22] on the embedding behavior of hard spherical and angular particles in ductile substrates. In both cases, the elastic rebound forces during impact could be sufficient to prevent embedding unless certain criteria were met. For angular particles, the directions of the normal and tangential components of elastic rebound forces remain constant due to the flat sides and sharp corners, and so long as the static friction forces between particle and substrate materials were sufficiently high, the particle will imbed [22]. For spherical particles, the constant curvature of the particle boundary leads to higher elastic rebound forces normal to the impact direction, and to embed the sphere must impact to a depth greater than its radius and be enveloped by material. Furthermore, spherical particles were not predicted to embed at all at impact angles perfectly normal to the substrate, as the elastic rebound forces were always higher than the friction forces retaining it [22]. Although this study does not consider the multi-particle impact scenario of cold spray, nor does it consider possible velocity differences between the angular and spherical particles, nonetheless the more stringent criteria for embedding spherical particles may be the cause for the lower spherical Al_2O_3 recovery seen here.

Microstructural examination revealed that the angular and spherical Al_2O_3 morphologies were retained after the cold spray process, although evidently some particle fracture occurred during deposition (see Figure 3). The porosity was below 2% for each coating. Microhardness measurements showed a linear relationship as a function of coating Al_2O_3 content, regardless of particle morphology (see Figure 4). Grain sizes in the aluminum matrix for all coatings showed a

ACCEPTED MANUSCRIPT

variation between roughly 200 nm and 5 µm; the arithmetic mean of several hundred grains on sample CS0 was 1.0 ± 0.8 µm (see Figure 5).

4 Dry sliding wear tests

4.1 Friction and transfer film behavior

The friction behavior during sliding wear tests was strongly influenced by the presence, concentration, and morphology of Al_2O_3 (see Figure 6). Sample CS0 exhibited a randomly fluctuating friction coefficient, varying between 0.45 and 1.2. Samples ANG10 and SPH3 showed less fluctuation behavior than CS0, while samples ANG22 and SPH11 showed the least fluctuation after an initial run-in period. Average friction data from all tests in the ranges of 0-50 cycles, 200-500 cycles, and 1000-2000 cycles were compiled as histograms (see Figure 7). Friction fluctuation corresponds to wide peaks, and in many cases peaks appear to be composed of multiple smaller peaks. As friction stabilizes, the peaks become narrower; this effect was clearly visible for samples ANG22 and SPH11 after 500 and 2000 cycles. Although the pattern for the friction spikes was semi-stochastic, the general friction behavior of samples as revealed through the histograms in Figure 7 was generally reproducible from test to test.

Behavior of third body material, monitored through in situ tribometry, also varied according to Al_2O_3 concentration and morphology (see Figure 8) [6, 16, 18]. Samples SPH3 and ANG10 showed similar behavior, where the transfer films were highly active; plowing and material transfer were clearly visible, as were plastic flow and material detachment. The holes left by material detachment were soon filled in by new transfer material. In some cases friction events could be directly correlated to events in the transfer film, while in other cases no change in the transfer film was visible. After 100 sliding cycles, samples SPH3 and ANG10 show large transfer films that take up most of the roughly 2 mm field of view (see Figure 8). The transfer films continued growing after this point and, by 500 sliding cycles, became larger than the field of view. Viewed ex situ, the SPH3 and ANG10 transfer film morphologies exhibited a maximum thicknesses of 90 - 100 µm at the prows, the leading edge of material transfer [6, 23]. In contrast

ACCEPTED MANUSCRIPT

to SPH3 and ANG10, in situ observations of samples SPH11 and ANG22 showed less transfer film activity after the initial transfer film formation. Activity such as hole formation and plastic flow was less obvious, if at all. The apparent area of transfer film of SPH11 remained relatively constant after the first 100 cycles, and by 500 cycles a central region opened where movement was visible, as evidenced through the in situ observations as well as the transfer film morphology. For ANG22, the center of the transfer film remained stable and present after 500 sliding cycles. For both SPH11 and ANG22, the thickness of transfer film viewed ex situ adhering to the sapphire did not exceed roughly 25 μm.

4.2 Wear track surface analysis

Surface analysis of wear tracks in an SEM revealed differences in the morphologies of third body material, which varied as a function of Al_2O_3 particle content, morphology, and sliding cycles (see Figure 9, left). After 50 cycles, samples SPH3, SPH11, and ANG10 showed some evidence of adhesive wear. This is characterized by smearing behavior, which results in tongue-shaped, layered structures on the surface of the wear track, and is commonly observed in aluminum tribology [6, 7, 24]. Sample ANG22, in contrast, showed the development of a coherent and smooth tribofilm after 50 cycles. Some regions of the SPH11 wear track also showed early stages of this development after 50 cycles, as evidenced by the smoother band of material in the center compared to the smeared material around it.

After 500 and 2000 cycles, surface analysis revealed a mix of adhesive wear and the development of third bodies (see Figure 9, middle and right). Sample SPH3 showed the beginning of tribofilm development after 500 cycles, and by 2000 cycles distinct patches of smooth tribofilm were present in the wear track, surrounded by regions of adhesive smearing and wear debris. SPH11 showed uniform coverage of a third body film after 500 cycles, present as half-cylinder regions about 100 μm wide, while after 2000 cycles these regions had flattened into a single coherent, smooth film. ANG10 showed continued evidence of adhesive wear after 500 and 2000 cycles, although tribofilm patches were visible in the wear track as well. Finally, ANG22 showed smooth, coherent tribofilms throughout testing, in keeping with previous studies [6, 7].

ACCEPTED MANUSCRIPT

Wear rates were dependent on Al_2O_3 concentration and morphology (see Figure 10). For all samples except ANG22, wear rates were highest at 50 cycles and lower at 500 and 2000 cycles. CS0, SPH3 and ANG10 had comparable wear rates, although the wear rate of SPH3 was slightly higher than that of CS0. Sample SPH11 consistently showed a lower wear rate than ANG10, in spite of similar Al_2O_3 concentrations. This effect was most prominent at 50 and 500 cycles, where the mean wear rate of SPH11 was roughly one third of that measured for ANG10, while after 2000 cycles it was roughly one half.

4.3 Wear track microstructural analysis and mechanical properties

Transverse cross-sections of a wear track of SPH3 after 500 sliding cycles revealed a mix of smooth and rough sections as was visible through surface analysis in Figure 9. In a smooth section shown in Figure 11(a) and 11(b), a coherent layer of ultrafine-grained Al (UFG Al) is present 3-10 µm thick. Underneath the UFG Al layer is large-grained aluminum (CG Al) appearing similar to that observed in the as-sprayed microstructure (see Figure 5). Similar to SPH11, the UFG Al runs up the side and partially envelops the spherical Al_2O_3 particle. In the rough region shown in Figure 11(c), an extruding region of material largely consisting of UFG Al is visible, with cracks visible between various sections.

Cross-sections of the near-surface material in ANG10 after 500 sliding cycles revealed deformed, ultrafine-grained material in a region 10 - 20 µm thick on top of the underlying coating which appears to be very little changed from the as-sprayed microstructure (see Figure 12). The deformed region consists of a mixture of ultrafine grained aluminum (UFG Al) and Al_2O_3 particles, some of which have been fragmented during the cold spray process or during sliding. Cracks are visible between layers of UFG Al and at the interface with the underlying coarse grained aluminum (CG Al), and these cracks often run to the corners of Al_2O_3 particles. The underlying CG Al microstructure shows grain refinement in roughly the top 5 µm.

Wear track microstructures from sample SPH11 after 500 sliding cycles (Figure 13) show the formation of a coherent, fine-grained layer across the entire wear track surface. Generally, this layer is roughly 5-10 µm thick, consisting of a UFG Al enveloping and partially spread along the top of Al_2O_3 particles. Below this layer is CG Al. Compared to the thick region of fine grained material of ANG10, few cracks are visible in sample SPH11, nor are any visible at the interface

ACCEPTED MANUSCRIPT

with the underlying first body. In the UFG layer, regions of dark contrast closer to the sliding surface contained elevated levels of oxygen.

Wear track microstructures of CS0 and ANG22 (not pictured) were examined in a previous study on cold sprayed Al-Al_2O_3 [6]. In that study it was observed that for CS0, layers of material 10-20 µm thick, exhibiting a mix of UFG and CG Al material were smeared on top of the underlying material in a similar fashion as ANG10 in Figure 12, and grain refinement was visible penetrating 5-10 µm deep into the underlying microstructure. For ANG22 (not pictured), a coherent UFG Al layer 2-5 µm deep with occasional fragments of Al_2O_3 was observed on top of a microstructure that appeared unchanged from the as-deposited state.

Nanoindentation on the UFG Al regions of the SPH3, ANG10, SPH11, and ANG22 wear tracks after 500 sliding cycles were found to be of elevated hardness compared to the CG Al regions (see Figure 14). For SPH11 and ANG22, the average hardness was roughly 3.8 GPa, which is very close to ANG22 wear track measurements in a previous work [6]. For both SPH3 and ANG10, the average hardness was around 2 GPa. This is slightly higher than previous measurements on CS0 which were on average around 1.5 GPa [6]. In all cases the UFG regions were harder than the underlying CG Al which had an average hardness of roughly 1 GPa, which is similar to that observed previously [6] and is the same as the hardness of the as-sprayed aluminum matrix prior to any wear testing.

5 Connections between Al_2O_3 particle morphology and the observed tribological behavior

For the tested Al-Al_2O_3 materials, contrasts were revealed in the friction, wear rates, transfer film behavior, and sub-surface microstructural changes that occurred during dry sliding. As tribological behavior is ultimately dictated by the behavior of third bodies at the sliding interface, it is clear through these results that both the morphology and the concentration of Al_2O_3 particles help drive the material transformations that create an “efficient" third body layer that lowers friction and wear.

Samples CS0, ANG10, and SPH3 exhibited the highest wear rates and the most unstable friction coefficients. Correspondingly, the third body behavior was very similar between ANG10 and SPH3. When viewed in situ, the third bodies were highly dynamic and exhibited frequent detachment of material; and when viewed ex situ, thick prow-shaped regions on the order of 100

ACCEPTED MANUSCRIPT

μm thick were observed (see Figure 8). These so-called Antler prows are associated with the active transfer of material from one surface to another, and it can lead to generation of new third body material [6, 23]. In the SPH3 and ANG10 wear tracks, surface analysis revealed evidence of adhesive wear, characterized by extensive plastic deformation causing a smearing effect. For ANG10, microstructural analysis showed that the adhesive wear led to thick third body layers settling in the bottom of the wear track, consisting of UFG Al and Al_2O_3 particles. For SPH3, the smooth regions of UFG Al show the beginning of a coherent third body layer forming, but the rough regions show that the process of wear debris formation was still very active. In spite of the different morphologies between the ANG10 and SPH3 third bodies, they were of comparable similar hardness values (Figure 14). The behavior of ANG10 and SPH3 in terms of friction, wear, and third body behavior is similar to that observed for CS0 in a previous study [6], indicating that the contents of 3 wt.% spherical Al_2O_3 and 10 wt.% angular Al_2O_3 were insufficient to greatly modify the tribological behavior in dry sliding.

Samples SPH11 and ANG22 exhibited the lowest wear rates and the most stable friction coefficients. The third body behavior viewed in situ for both samples was far less active than for the SPH3 and ANG10, and ex situ analysis revealed thin transfer films adhering to the counterfaces without any visible Antler prows. Surface analysis of SPH11 and ANG22 revealed wear tracks that were relatively smooth, and in cross-sections SPH11 revealed the formation of smooth, coherent third body layers 5-10 μm thick of UFG Al that partially enveloped the spherical Al_2O_3 particles. The microstructures of SPH11 are quite comparable to those observed in ANG22 [6], where a consistent, coherent third body layer consisting of UFG Al and fragments of Al_2O_3 was formed. Furthermore, the SPH11 and ANG22 third body layers were of very similar hardness values of roughly 3.8 GPa. Although the wear rates were lower for ANG22 than for SPH11, and the friction coefficient of SPH11 was more unstable than that of ANG22 at early sliding cycles, the tribological processes were nonetheless similar between the two samples after the initial running-in period, which was longer for SPH11 than ANG22.

Therefore to achieve lower wear rates and friction, the most effective third body for this system consisted of a single coherent layer of UFG Al that is between 2 and 10 μm thick, is relatively free of cracks, and has a hardness of roughly 3.8 GPa. Third body layers of these criteria formed only for samples SPH11 and ANG22. The formation of this layer was linked to a coupling of

ACCEPTED MANUSCRIPT

sufficiently high concentration of Al_2O_3 particles and of the particle morphology. As aluminum is transferred and smeared across Al_2O_3 particles, strain localization and high strain gradients in the vicinity of the hard particles results in enhanced dislocation formation and grain refinement. This effect of localized grain refinement in the vicinity of hard particles has been observed in severe plastic deformation (SPD) process such as high pressure torsion [25-27]. The increase in hardness is linked to the extreme amount of grain refinement and work hardening in this layer, as well as tribo-oxidation. Kim et al. studied the oxygen contained in wear debris formed after dry sliding on pure aluminum and found that it could be present as a metastable oxygen solid solution, formed through the extreme plastic deformation processes occurring at the sliding interface [28]. Although a quantitative analysis of oxygen content in the mechanically mixed material was not carried out in this study, a previous study by the authors on the third body material of a similar material system found significant oxygen content, yet it was lower than that of stoichiometric Al_2O_3 [6].

SPH11 and ANG10 had comparable Al_2O_3 contents and microhardness values; yet at this concentration of Al_2O_3, the most effective third body layer formed only in the case of the spherical Al_2O_3 morphology. Reinforcement particle morphology in Al-MMC materials has been previously shown to strongly influence tribological behavior. Tribological studies on Al-Si alloys, which are considered in situ Al-MMC materials and are frequently used in tribological applications, have found that the sphericity of the Si phase can have a strong effect on wear rates. Elmadagli et al. found that in Al-Si alloys, heat treatments could cause the as-cast acicular Si morphology to spheroidize [29]. This spheroidization step was attributed to a reduction of wear rates by roughly 30%. Yang et al. measured similar reductions in wear rates after adding alloy elements promoting Si spheroidization, and partly attributed this to the observation that cracks in angular Si particles could propagate into the third body layer and lead to detachment of wear debris [30]. Such third body instability would lead to greater wear debris generation, and this is likely the case in the present study as well.

Further study of literature on the deformation behavior of Al-MMCs offers a partial explanation for the influence of particle morphology. When Al-MMC materials are deformed, whether in tension, compression, or shear, the plastic flow of the matrix is constrained in the vicinity of stiff reinforcement particles [31]. The resulting stress concentration induces strengthening to the

ACCEPTED MANUSCRIPT

composites compared to the unreinforced matrix material [32], and the microstructural changes responsible for this strengthening have been observed in tensile loading [33] and in tribological scenarios [34]. However, reinforcement morphology strongly influences the constrained plastic strain fields in the matrix, with severe stress concentration in the regions close to sharp corners of angular particles [31]. Although angular reinforcements can result in higher strength in tensile loading compared to spherical, they also lead to reduced ductility due to enhanced particle fracture and matrix damage accumulation at stress concentration sites [33]. It follows that in a tribological scenario like the present study, it is possible that the reduced ductility and damage accumulation at the sharp corners of angular particles act to allow material detachment during sliding, more readily generating wear debris and clearing away regions of MML. This would be closely linked to spikes in the friction coefficient and activity in the transfer film, which were associated with higher overall wear rates.

Therefore for this sliding system, two competing processes occurred in the vicinity of hard particles: third body formation through strain localization and oxidation, and third body disturbance/removal contributing to the detachment of wear debris. For sample SPH3, some smooth patches of third bodies formed in the wear track, but the amount of Al_2O_3 was insufficient to prevent its disturbance and removal as wear debris. For ANG10 and SPH11, with similar concentrations of particles, the sharp corners of the angular Al_2O_3 in ANG10 promoted crack formation and detachment. The stability of the third body layer for SPH11 allowed it to contribute to work hardening and oxidation, leading to its elevated hardness. ANG22 had such high quantities of angular Al_2O_3 that the third body formation process dominated over the detachment process, leading to the elevated hardness and stability of the third body layer similar to that of SPH11, but at a lower wear rate.

6 Conclusions

The present study has explored the influence of Al_2O_3 morphology on the deposition behavior and dry sliding wear behavior of cold sprayed Al-Al_2O_3 using admixed feedstock powders. During cold spray deposition, significantly less spherical Al_2O_3 compared to angular Al_2O_3 was recovered at similar feedstock concentrations. Coating microhardness was found to depend only on the concentration of Al_2O_3 in the coating and not on the particle morphology.

ACCEPTED MANUSCRIPT

In dry sliding wear tests, coatings with 3 wt.% spherical (SPH3) and 10 wt.% angular (ANG10) Al_2O_3 were found to have similar wear rates as unreinforced cold sprayed pure Al and similarly high, unstable friction coefficients. Coatings of 11 wt.% spherical (SPH11) and 22 wt.% Al_2O_3 (ANG22) were found to have lower wear rates and lower, more stable friction coefficients compared to the coatings of lower Al_2O_3 content. Tribological mechanisms were observed through in situ tribometry and ex situ analysis of worn material. Samples exhibiting high wear rates and high friction were found to have high levels of material flow at the sliding interface, and this resulted in disordered, inhomogeneous microstructures in the third body material in the wear track. Samples exhibiting low wear rates and low friction were found to have stable third body material present in a thin, hardened, coherent layer of fine-grained material that was highly oxidized. The “critical" concentration of Al_2O_3 required to form this layer was strongly dependent on the morphology of the Al_2O_3 particles, with less spherical Al_2O_3 being needed compared to angular.

Acknowledgments

The authors gratefully acknowledge the financial support from the Canadian Foundation for Innovation (CFI) project No. 8246 for the cold spray equipment, the CFI Leader's Opportunity Fund project No. 13029 for the in situ tribometer and nanoindentation equipment, and the Natural Sciences and Engineering Research Council (NSERC) Discovery Grants Program for the operational funding of this project. Thanks are also due to Tekna Inc. of Sherbrooke, QC for providing the spherical Al_2O_3 powders. JMS acknowledges partial financial support from the Rio Tinto Alcan Graduate Fellowships program.

References

[1] T.W. Clyne and P.J. Withers. An Introduction to Metal Matrix Composites, Fabrication Processes, pages 318-360. Cambridge University Press, Cambridge, 1993.

[2] R.L. Deuis, C. Subramanian, and J.M. Yellup. Dry Sliding Wear of Aluminium Composites-A Review. Composites Science and Technology, 57:415-435, 1997.

[3] B. Venkataraman and G. Sundararajan. The sliding wear behaviour of Al-SiC particulate composites - I. Macrobehaviour. Acta Materialia, 44(2):451-460, 1996.

ACCEPTED MANUSCRIPT

[4] A.T. Alpas and J. Zhang. Effect of Microstructure (Particulate Size and Volume Fraction) and Counterface Material on the Sliding Wear Resistance of Particulate-Reinforced Aluminum Matrix Composites. Metallurgical and Materials Transactions A, 25A:969-983, 1994.

[5] Eric Irissou, Jean-Gabriel Legoux, Bernard Arsenault, and Christian Moreau. Investigation of Al-Al_2O_3 Cold Spray Coating Formation and Properties. Journal of Thermal Spray Technology, 16(5-6):661-668, 2007.

[6] J. Michael Shockley, S. Descartes, E. Irissou, J.-G. Legoux, and R. R. Chromik. Third body behavior during dry sliding of cold-sprayed al-Al_2O_3 composites: In situ tribometry and microanalysis. Tribology Letters, 54:191-206, 2014.

[7] K. Spencer, D.M. Fabijanic, and M.-X. Zhang. The use of Al-Al_2O_3 cold spray coatings to improve the surface properties of magnesium alloys. Surface & Coatings Technology, 204:336-344, 2009.

[8] Yongshan Tao, Tianying Xiong, Chao Sun, Huazi Jin, Hao Du, and Tiefan Li. Effect of Al-Al_2O_3 on the properties of cold sprayed Al-Al_2O_3 composite coatings on AZ91D magnesium alloy. Applied Surface Science, 256(1):261 - 266, 2009.

[9] U.S. Department of Defense, U.S. Army Research Laboratory: Materials Deposition, Cold Spray, Standard MIL-STD-3021, 2008.

[10] Hamid Assadi, Frank G□artner, Thorsten Stoltenhoff, and Heinrich Kreye. Bonding mechanism in cold gas spraying. Acta Materialia, 51:4379-4394, 2003.

[11] F. Gartner, T. Stoltenhoff, T. Schmidt, and H. Kreye. The cold spray process and its potential for industrial applications. Journal of Thermal Spray Technology, 15(2):223-232, 2006.

[12] Eric Irissou, Jean-Gabriel Legoux, Anatoly Ryabinin, Bertrand Jodoin, and Christian Moreau. Review on Cold Spray Process and Technology: Part I-Intellectual Property. Journal of Thermal Spray Technology, 17(4):495-516, 2008.

[13] V.K. Champagne. The Cold Spray Materials Deposition Process: Fundamentals and Applications. Woodhead Publishing Limited, Cambridge, 2007.

ACCEPTED MANUSCRIPT

[14] A. Papyrin, V. Kosarev, K.V. Klinkov, A. Alkhimov, and V.M. Fomin. Cold Spray Technology. Elsevier, Oxford, 2006.

[15] Victor K. Champagne. The Repair of Magnesium Rotorcraft Components by Cold Spray. Journal of Failure Analysis and Prevention, 8:164-175, 2008.

[16] J.M. Shockley, H.W. Strauss, R.R. Chromik, N. Brodusch, R. Gauvin, E. Irissou, and J.-G. Legoux. In situ tribometry of cold-sprayed Al-Al_2O_3 composite coatings. Surface and Coatings Technology, 215:350-356, 2013.

[17] Maurice Godet. The third-body approach: a mechanical view of wear. Wear, 100:437-452, 1984.

[18] R. R. Chromik, H. W. Strauss, and T. W. Scharf. Materials phenomena revealed by in situ tribometry. JOM, 64(1):35-43, 2012.

[19] W.C. Oliver and G.M. Pharr. An improved technique for determining hardness and elastic modulus using load and displacement sending indentation experiments. Journal of Materials Research, 7(6):1564-1586, 1992.

[20] A. Sova, D. Pervushin, and I. Smurov. Development of multimaterial coatings by cold spray and gas detonation spraying. Surface & Coatings Technology, 205:1108-1114, 2010.

[21] Qiang Wang, Kevin Spencer, Nick Birbilis, and Ming-Xing Zhang. The influence of ceramic particles on bond strength of cold spray composite coatings on AZ91 alloy substrate. Surface and Coatings Technology, 205(1):50 - 56, 2010.

[22] H. Getu, J.K. Spelt, and M. Papini. Conditions leading to the embedding of angular and spherical particles during the solid particle erosion of polymers. Wear, 292-293:159-168, 2012.

[23] Morton Antler. Processes of Metal Transfer and Wear. Wear, 7:181-203, 1964.

[24] H.-J. Kim, A. Emge, S. Karthikeyan, and D.A. Rigney. Effects of tribooxidation on sliding behavior of aluminum. Wear, 259:501-505, 2005.

ACCEPTED MANUSCRIPT

[25] P.J. Apps, J.R. Bowen, and P.B. Prangnell. The effect of coarse second-phase particles on the rate of grain refinement during severe deformation processing. Acta Mat, 51:2811-2822, 2003.

[26] I. Gutierrez-Urrutia, M.A. Munoz-Morris, and D.G. Morris. Contribution of microstructural parameters to strengthening in an ultrafine-grained Al-7Si alloy Acta Materialia, 55:1319-1330, 2007.

[27] I. Gutierrez-Urrutia, M.A. Munoz-Morris, I. Puertas, C. Luis, and D.G. Morris. Influence of processing temperature and die angle on the grain microstructure produced by severe deformation of an Al-7Si alloy, Materials Science and Engineering A, 475:268-278, 2008.

[28] Hong Jin Kim, Wolfgang Windl, and D.A. Rigney. Structure and chemical analysis of aluminium wear debris: Experiments and ab initio simulations. Acta Materialia,55:6489-6498, 2007.

[29] M. Elmadagli, T. Perry, and A.T. Alpas. A parametric study of the relationship between microstructure and wear resistance of Al-Si alloys. Wear, 262:79-92, 2007.

[30] C.-Y. Yang, S.-L. Lee, C.-K. Lee, and J.C. Lin. Effects of Sr and Sb modifiers on the sliding wear behavior of a357 alloy under varying pressure and speed conditions. Wear, 261:1348-1358, 2006.

[31] Y.-L. Shen. Constrained Deformation of Materials. Springer, 2010.

[32] T. CHRISTMAN, A. NEEDLEMAN, and S. SURESH. An experimental and numerical study of deformation in metal-ceramic composites. Acta Metallurgica, 37(11):3029-3050, 1989.

[33] S.G. Song, N. Shi, G.T. Gray III, and J.A. Roberts. Reinforcement shape effects on the fracture behavior and ductility of particulate-reinforced 6061-Al matrix composites. METALLURGICAL AND MATERIALS TRANSACTIONS A, 27A:3739-3746, 1996.

[34] W.M. Rainforth. Microstructural evolution at the worn surface: a comparison of metals and ceramics. Wear, 245:162-177, 2000.

ACCEPTED MANUSCRIPT

Sample Designation	Al_2O_3 Particle Morphology	Al_2O_3 in Feedstock Powder (wt.%)
CS0	n/a	0
ANG10	Angular	10
ANG22	Angular	50
SPH3	Spherical	10
SPH11	Spherical	50

Table 1 - Sample designations and Al_2O_3 content in the feedstock powder. Sample designations refer to the morphology and amount of Al_2O_3 recovered in the coating (see Figure 2).

ACCEPTED MANUSCRIPT

ACCEPTED MANUSCRIPT

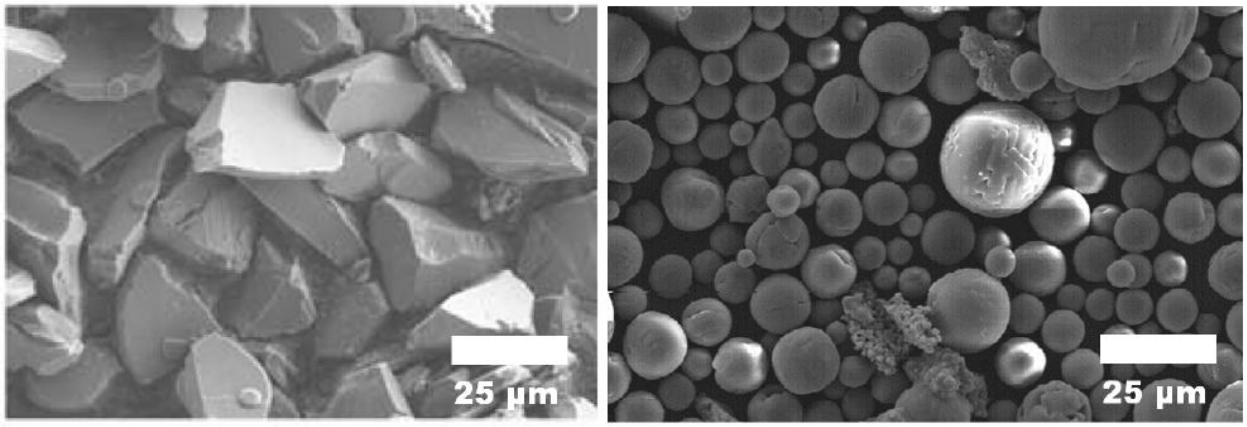

Figure 1 - Feedstock Al_2O_3 powders before admixing. Left: angular Al_2O_3 (from [5]). Right: spherical Al_2O_3.

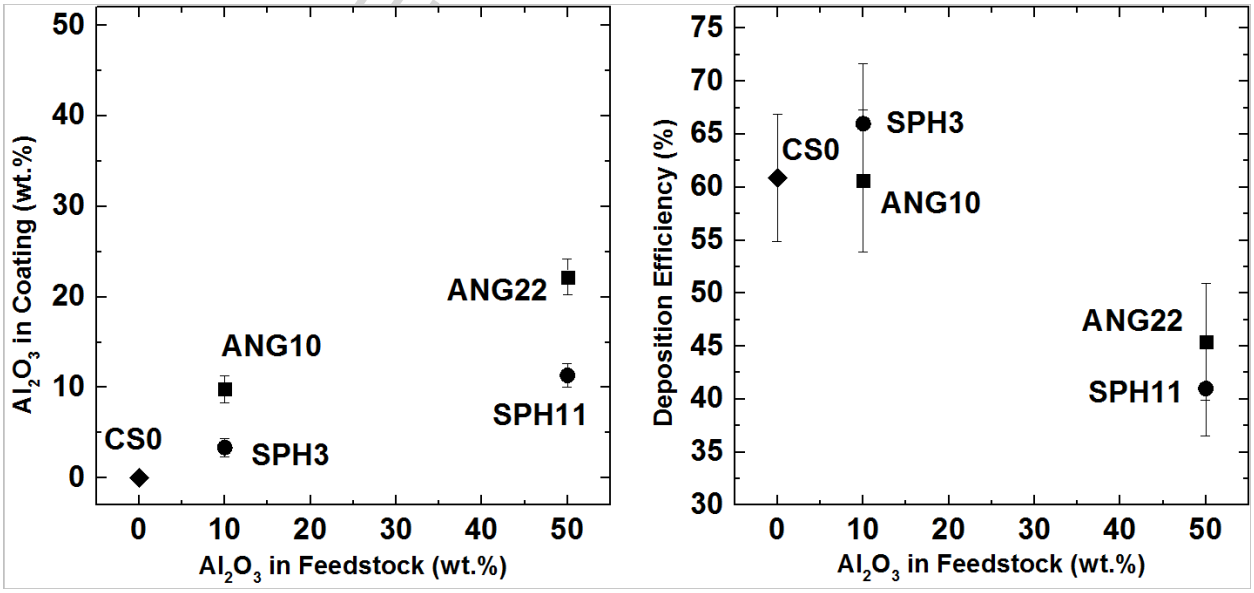

Figure 2 - Recovery of Al_2O_3 (left) and deposition efficiency (right) of the sprayed coatings.

ACCEPTED MANUSCRIPT

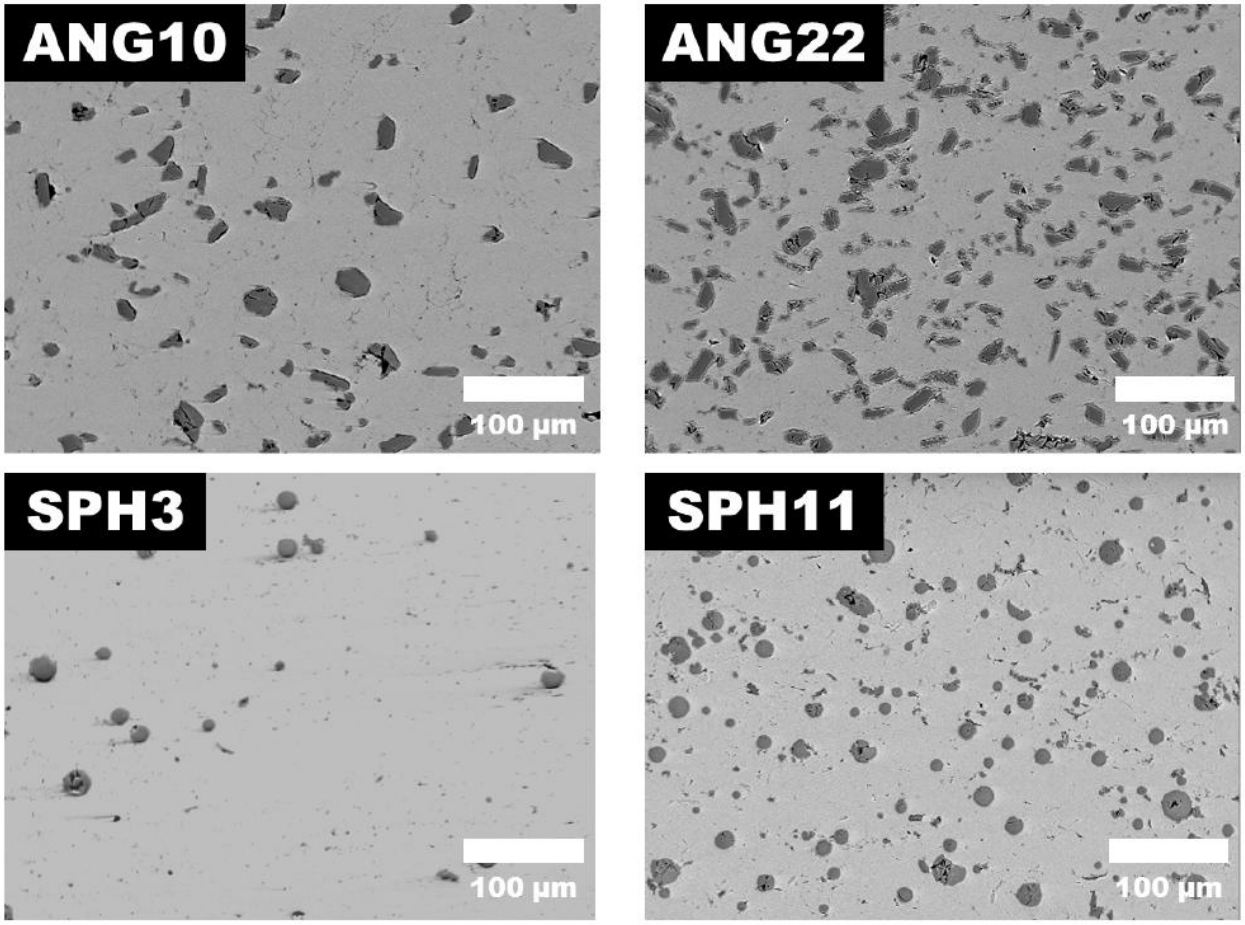

Figure 3 - Cross-sections of the as-sprayed microstructures viewed roughly 1 mm below the top surface of the deposits.

ACCEPTED MANUSCRIPT

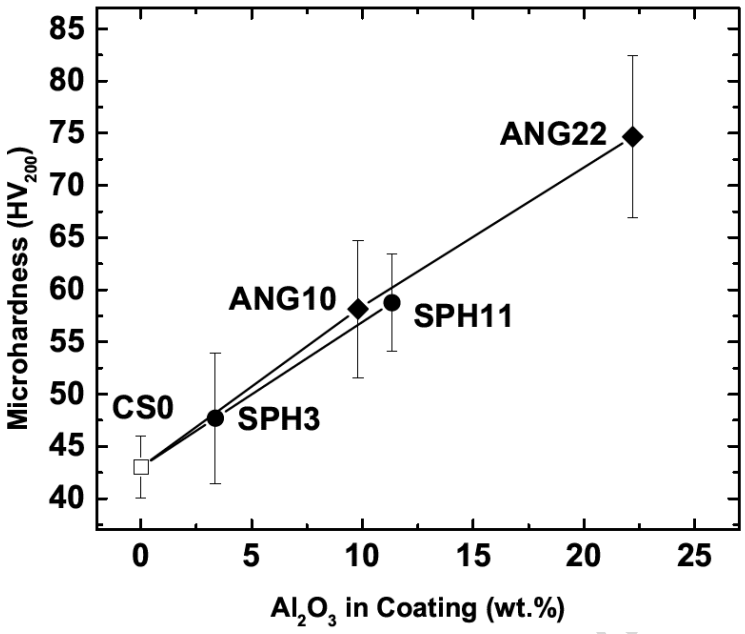

Figure 4 - Microhardness measurements of the tested coatings.

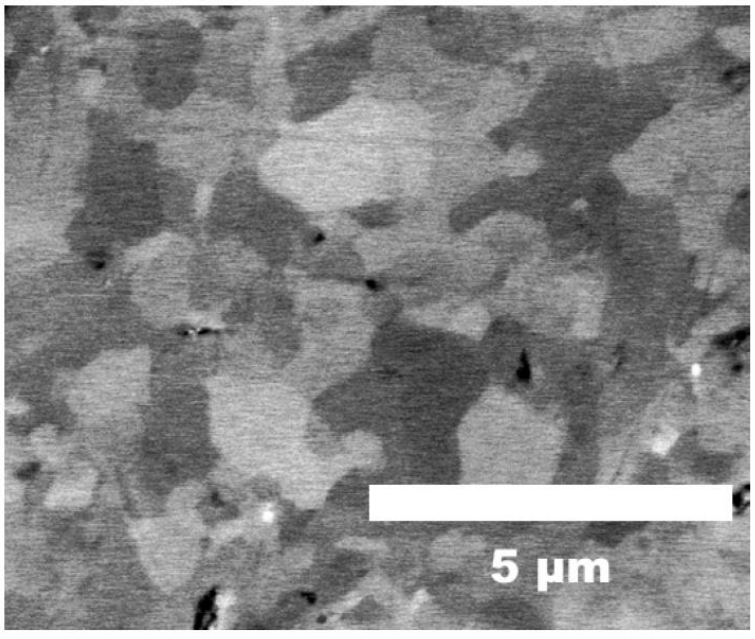

Figure 5 - Representative ECCI micrograph of typical as-sprayed grain sizes in the aluminum matrix for all samples prior to sliding wear testing.

ACCEPTED MANUSCRIPT

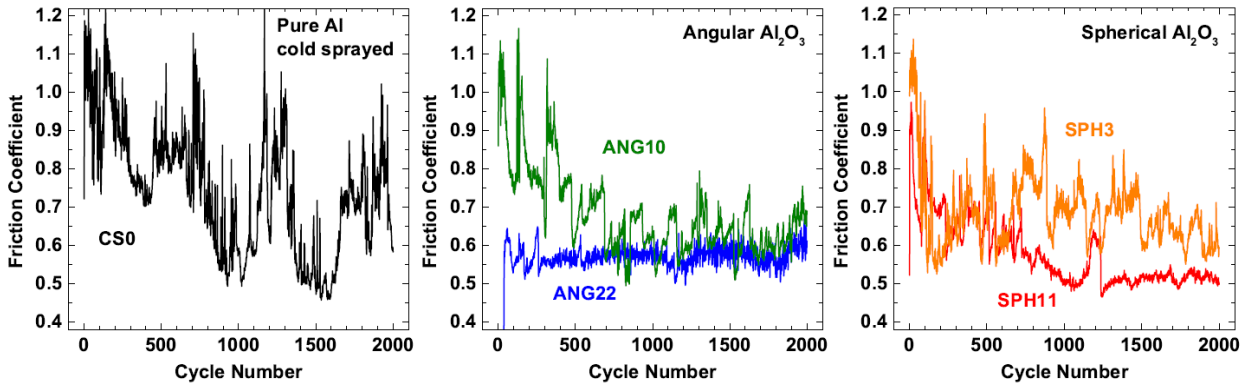

Figure 6 - Representative plots of average friction coefficient plotted versus cycle number: pure cold sprayed Al (left), angular Al_2O_3 samples (middle), and spherical Al_2O_3 samples (right).

ACCEPTED MANUSCRIPT

ACCEPTED MANUSCRIPT

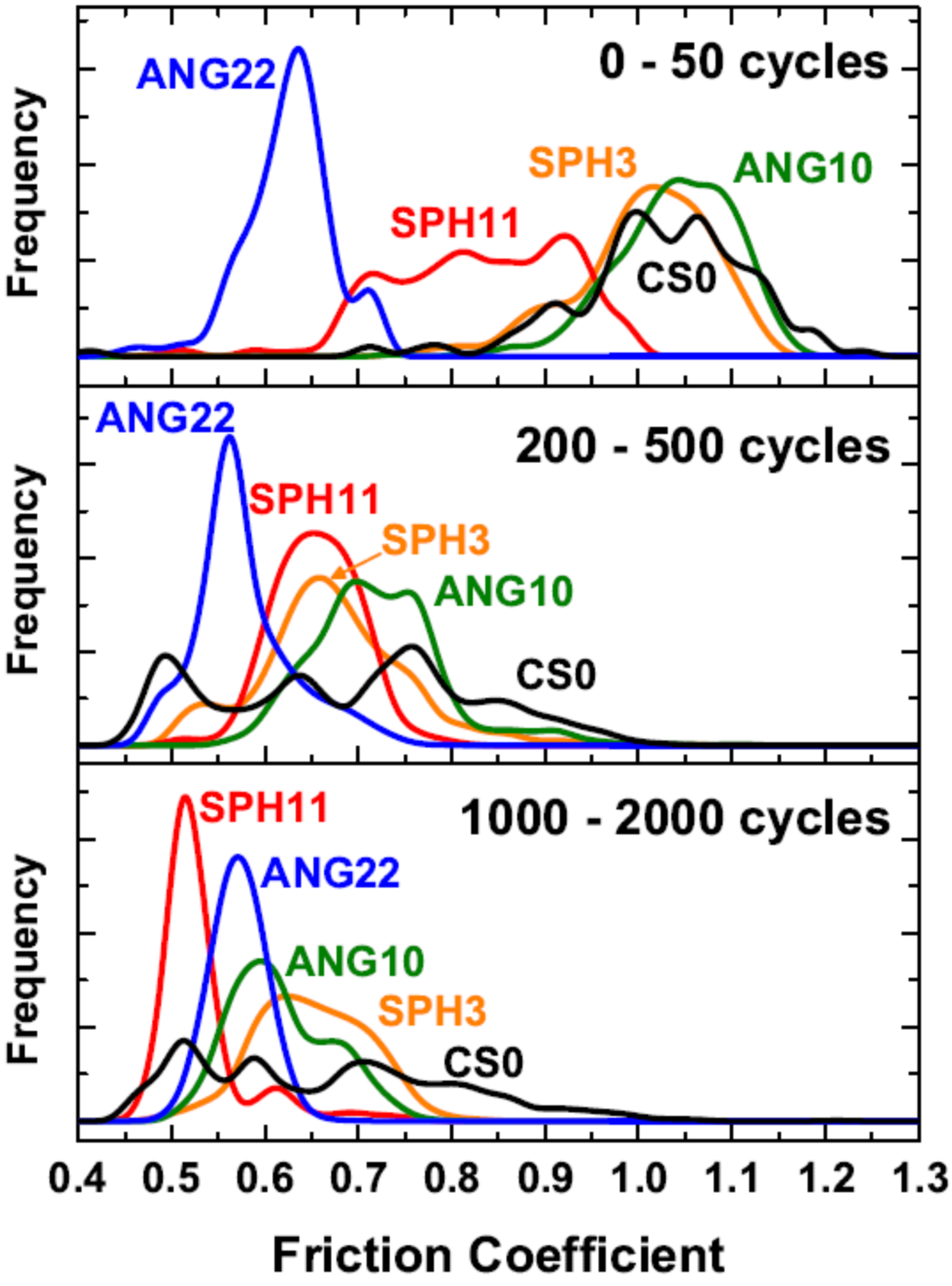

1

2 Figure 7 - Friction plotted as frequency distributions; a spline fit was used plot the binned data.

ACCEPTED MANUSCRIPT

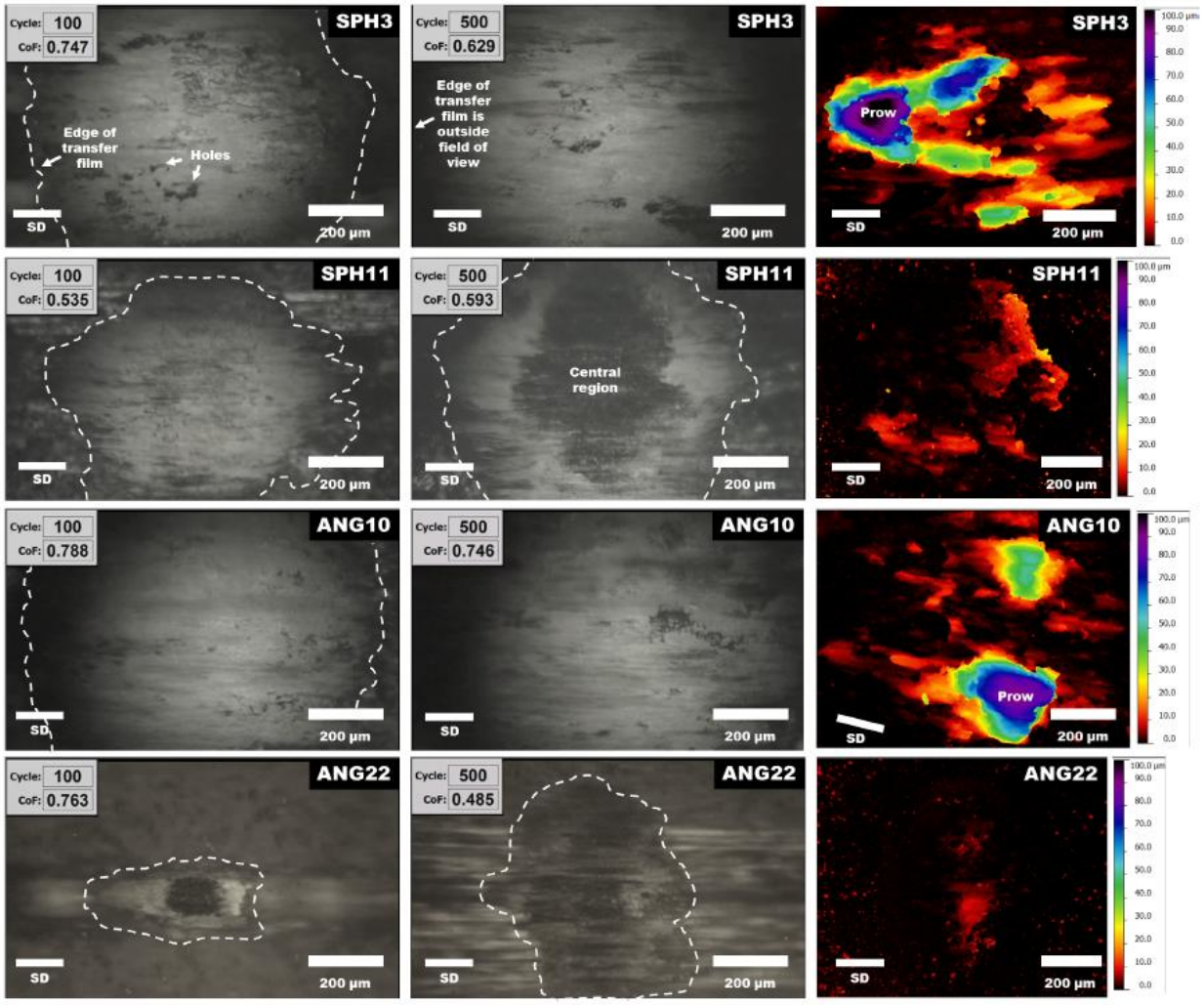

Figure 8 - Left and middle: Transfer films observed in situ at 100 and 500 sliding cycles. Transfer film borders are marked where visible. Right: morphologies of transfer films adhering to the counterface after 500 cycles. “SD" indicates sliding direction.

ACCEPTED MANUSCRIPT

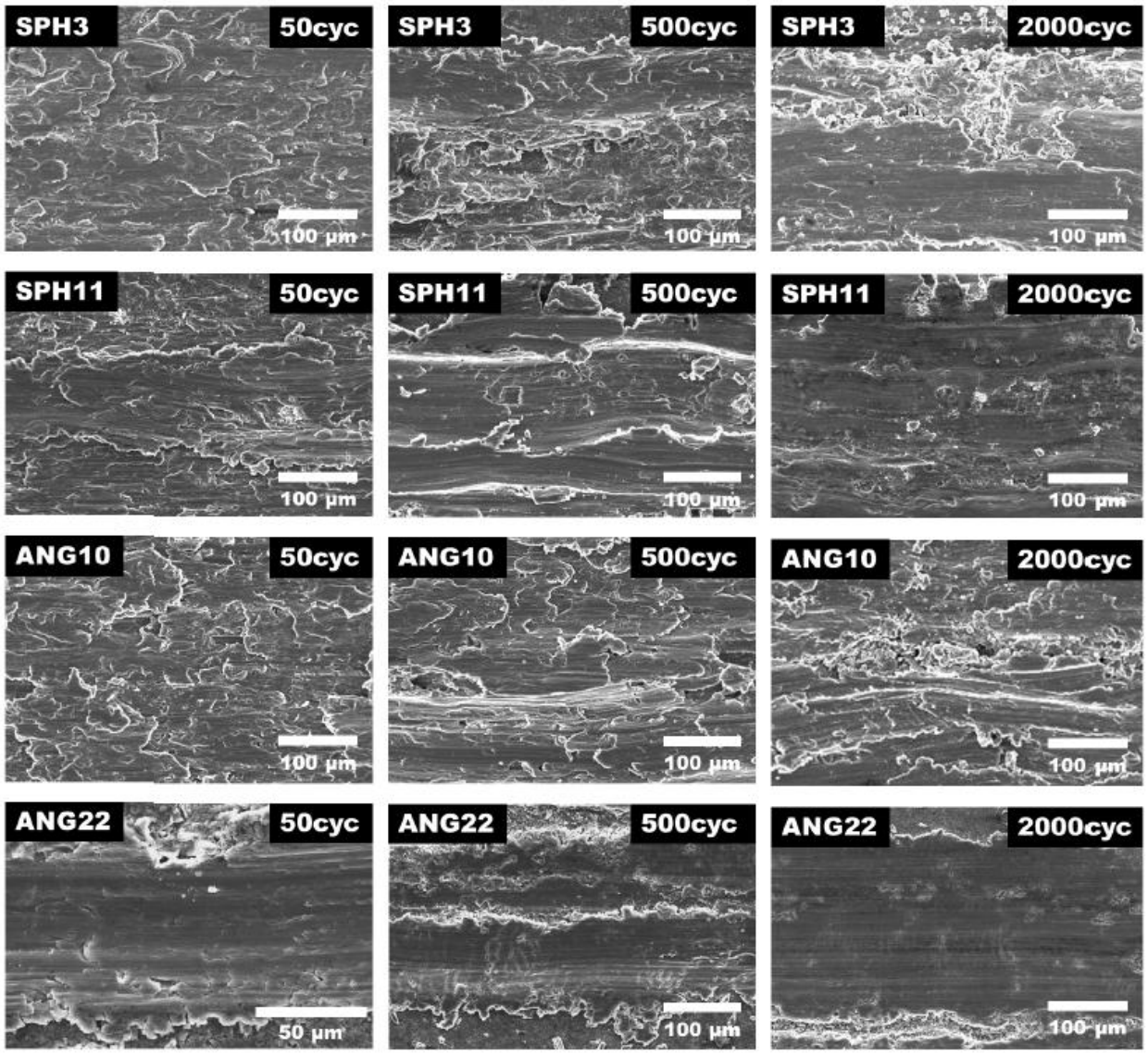

Figure 9 - Surface features of the wear tracks after 50, 500, and 2000 sliding cycles. Sliding direction is horizontal.

ACCEPTED MANUSCRIPT

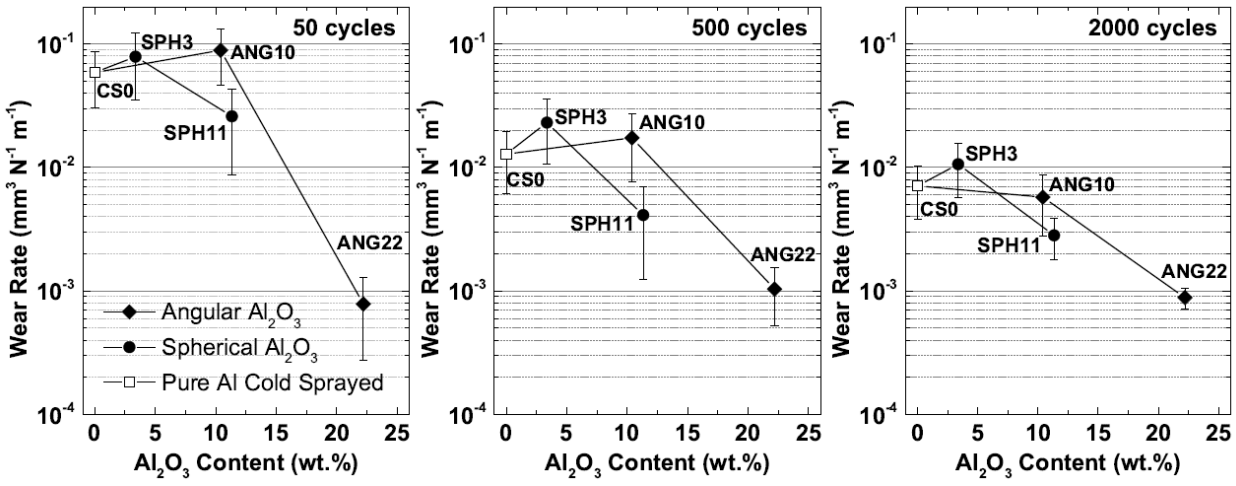

Figure 10 - Volumetric wear rate plotted versus cycle number. The error bars show plus and minus one standard deviation.

ACCEPTED MANUSCRIPT

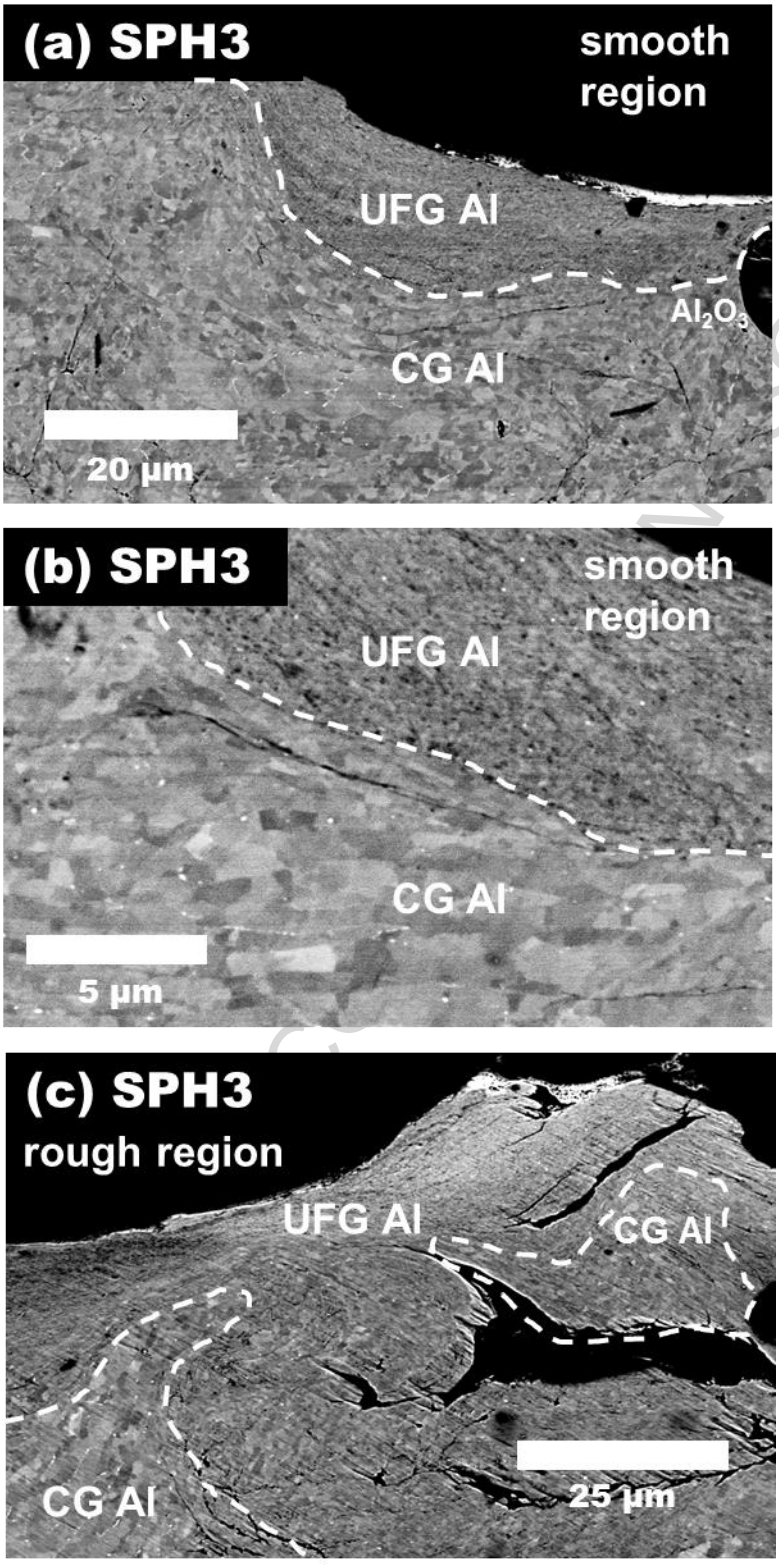

Figure 11 - Cross-sections of the near-surface microstructures after 500 sliding cycles for sample SPH3.

ACCEPTED MANUSCRIPT

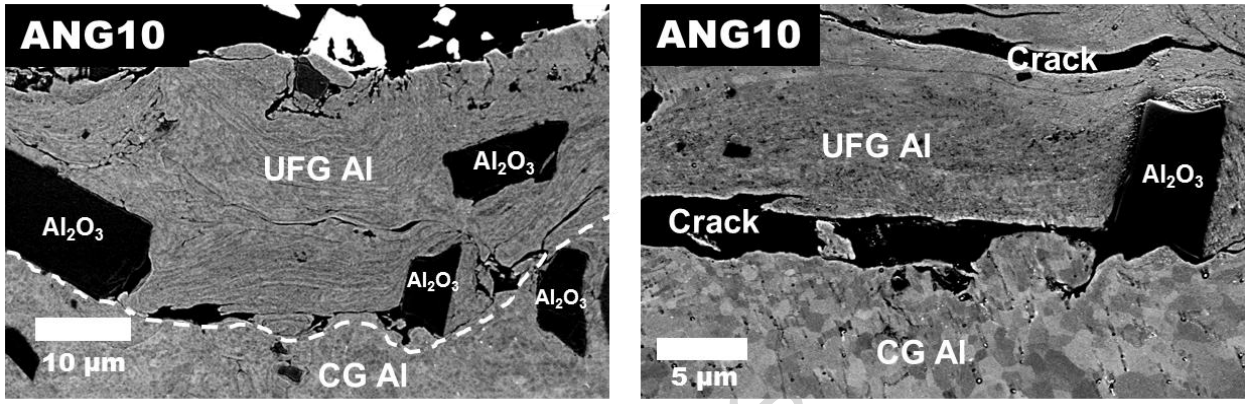

Figure 12 - Cross-sections of the near-surface microstructures after 500 sliding cycles for sample ANG10.

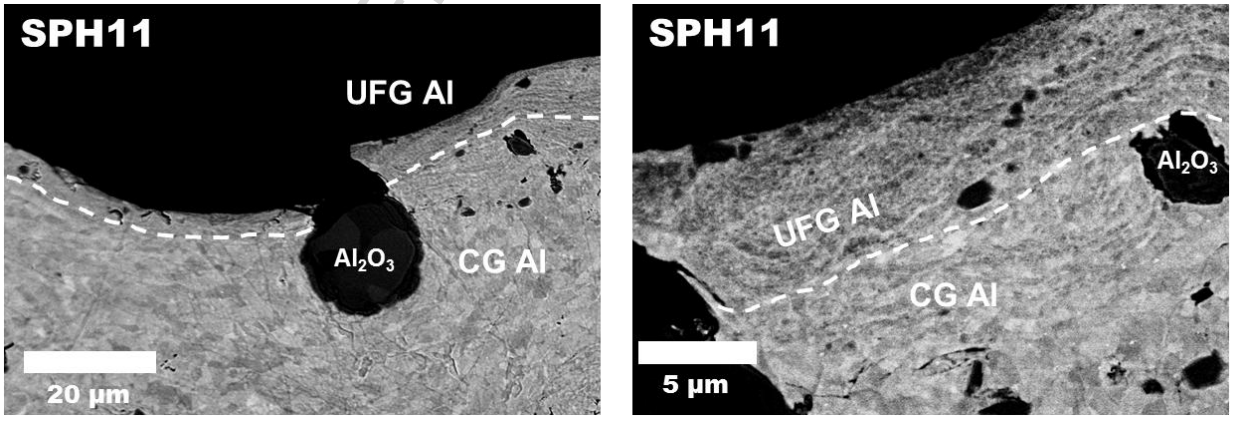

Figure 13 - Cross-sections of the near-surface microstructures after 500 sliding cycles for sample SPH11.

ACCEPTED MANUSCRIPT

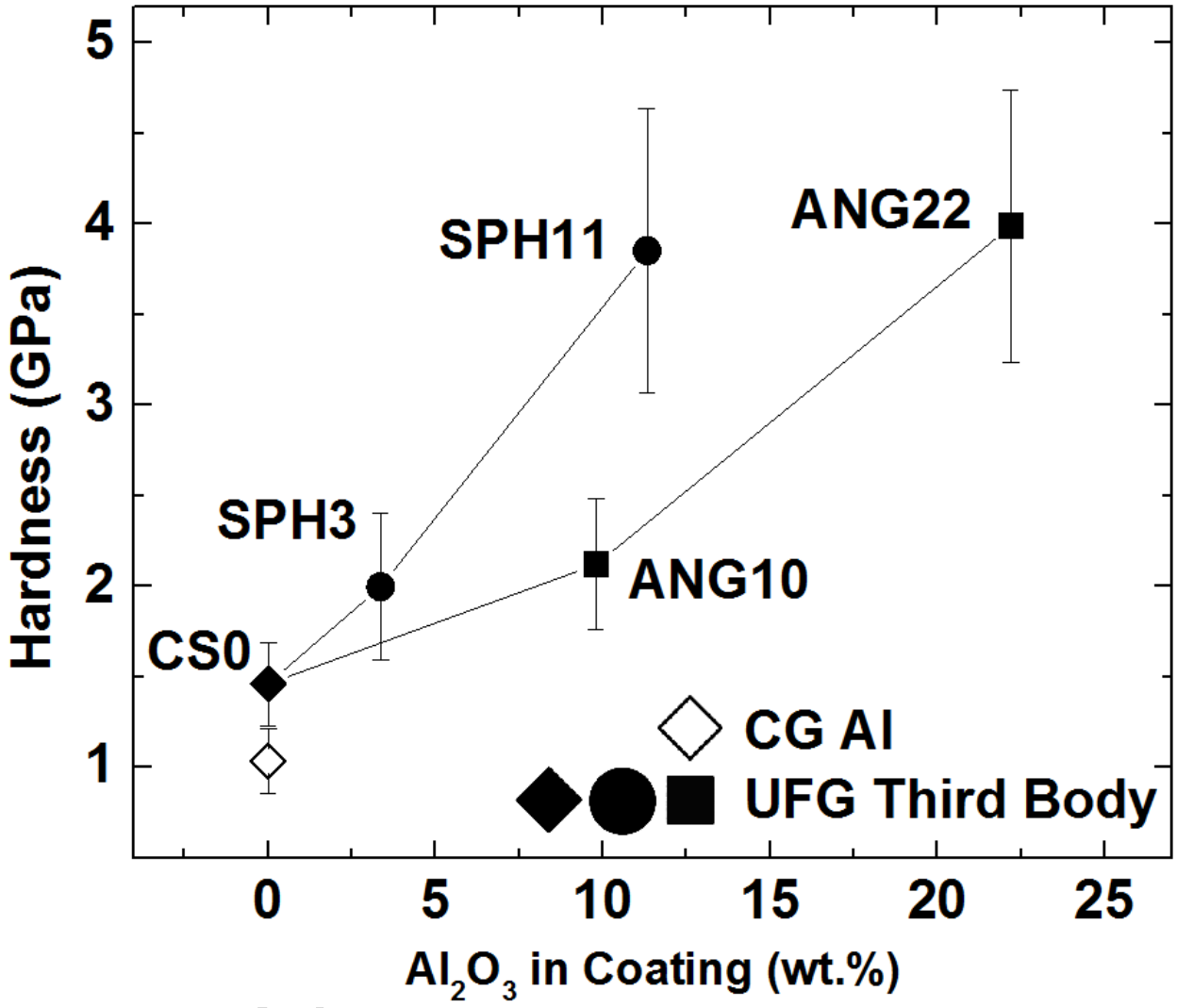

Figure 14 - Hardness of CG Al and UFG material (from Figures 12, 13, and 11) in the tested samples. Data for CS0 UFG Al was taken from a previous study by the authors [6].

ACCEPTED MANUSCRIPT

Highlights from "The influence of Al_2O_3 particle morphology on the coating formation and dry sliding wear behavior of cold sprayed Al-Al_2O_3 composites" :

- Al-Al_2O_3 coatings were cold sprayed with either angular or spherical Al_2O_3
- Al_2O_3 recovery was greater for angular than spherical morphologies
- Dry sliding wear test were performed on the coatings
- Spherical Al_2O_3 led to a lower wear rate and more stable friction than angular
- Tribological behaviors were linked to the evolution of third body material

ACCEPTED MANUSCRIPT